Diacylglycerol kinase ε regulates seizure susceptibility and long-term potentiation through arachidonoyl–inositol lipid signaling

Elena B. Rodriguez de Turco*, Wen Tang†, Matthew K. Topham†, Fumio Sakane†, Victor L. Marcheselli*, Chu Chen*, Akinobu Taketomi†, Stephen M. Prescott†‡, and Nicolas G. Bazan*‡

*Neuroscience Center of Excellence and Department of Ophthalmology, Louisiana State University Health Sciences Center, New Orleans, LA 70112; and †The Huntsman Cancer Institute, University of Utah, Salt Lake City, UT 84112

Edited by Solomon H. Snyder, Johns Hopkins University School of Medicine, Baltimore, MD, and approved February 13, 2001 (received for review November 9, 2000)

Arachidonoyldiacylglycerol (20:4-DAG) is a second messenger derived from phosphatidylinositol 4,5-bisphosphate and generated by stimulation of glutamate metabotropic receptors linked to G proteins and activation of phospholipase C. 20:4-DAG signaling is terminated by its phosphorylation to phosphatidic acid, catalyzed by diacylglycerol kinase (DGK). We have cloned the murine DGKε gene that showed, when expressed in COS-7 cells, selectivity for 20:4-DAG. The significance of DGKε in synaptic function was investigated in mice with targeted disruption of the DGKε. DGK$\varepsilon^{-/-}$ mice showed a higher resistance to eletroconvulsive shock with shorter tonic seizures and faster recovery than DGK$\varepsilon^{+/+}$ mice. The phosphatidylinositol 4,5-bisphosphate-signaling pathway in cerebral cortex was greatly affected, leading to lower accumulation of 20:4-DAG and free 20:4. Also, long-term potentiation was attenuated in perforant path–dentate granular cell synapses. We propose that DGKε contributes to modulate neuronal signaling pathways linked to synaptic activity, neuronal plasticity, and epileptogenesis.

Arachidonic acid (20:4), inositol lipid-derived diacylglycerols (DAGs), and other bioactive lipids (i.e., platelet-activating factor, PAF) have been implicated in neuronal plasticity, ischemic brain damage, and epilepsy (1–4). These potent bioactive lipids are generated by the excitatory neurotransmitter glutamate through the activation of phospholipase A_2 (PLA_2) and phospholipase C (PLC) signaling pathways. Increased postsynaptic calcium permeation through channels gated by *N*-methyl-D-aspartate (NMDA)-glutamate receptor leads to activation of signaling via cystolic PLA_2 ($cPLA_2$) and 20:4 release. Activation of metabotropic receptors (mGluRs), coupled to G proteins and PLC, increases DAG concentration due to the hydrolysis of phosphatidylinositol 4,5-bisphosphate (PIP_2) (5). A subsequent increase in DAG pool size follows as a result of phospholipase D (PLD)-catalyzed hydrolysis of phosphatidylcholine to phosphatidic acid (PA) and its conversion to DAG (6, 7). The early and late DAG peaks are temporally dissociated, and their fatty acid composition is different (8, 9). Inositol phospholipids are enriched in arachidonate at the *sn2* position of the glycerol backbone, whereas in phosphatidylcholine this position is occupied mainly by monounsaturated fatty acid chains (i.e., oleic acid, 18:1n-9) (7).

20:4-DAG activates protein kinase C (PKC) *in vitro* (6) and plays second messenger functions *in vivo* (7, 10). Moreover, there is evidence that targets of DAG can distinguish between different DAG species (11). Thus, the distinct fatty acid composition of inositol phospholipids in neuronal cell signaling may be important for the maintenance of cellular functional integrity. It is not entirely clear how inositol lipid species become enriched in arachidonate. Enzymes responsible for inositol lipid synthesis may selectively use 20:4-containing lipids as substrates (12). DAG kinase ε (DGKε), which selectively phosphorylates 20:4-DAG to generate PA (11, 13), is one candidate. Eight other mammalian DGKs with no significant selectivity have been identified (14).

We reasoned that targeted deletion of the DGKε gene would be an effective approach to determine whether DGKε contributes to the arachidonate enrichment and, if so, what functional consequences insofar as seizure responses and long-term potentiation (LTP) occur when its activity is lost. The 20:4-DAG signal generated from mGluR-activated PIP_2-PLC pathway is switched off by DGKε that generates PA. This, in turn, is used for the synthesis of phosphatidylinositol and the replenishment of the precursor by phosphorylations to phosphatidylinositol 4-phosphate (PIP) and PIP_2. Activation of inositide lipid signaling through mGluR1 and PKC is involved in synaptic plasticity such as in learning, memory, LTP (15–20), and long-term depression (21). Moreover, alterations of this signaling have been implicated in neurological and psychiatric diseases such as epilepsia, Alzheimer's disease, and depression (2, 22, 23). To define the significance of the 20:4–inositol lipids in seizures and LTP, we used mice deficient in DGKε (DGK$\varepsilon^{-/-}$) and found this cycle to be down-regulated, resulting in a reduced ECS-induced accumulation of 20:4-DAG. Moreover, DGK$\varepsilon^{-/-}$ mice were more resistant to ECS and displayed attenuated LTP in perforant path–dentate granular cell synapses. These findings support the notion that 20:4-inositol lipid signaling is involved in neural responses during seizures and in hippocampal synaptic plasticity.

Materials and Methods

Isolation of Murine DGK cDNA and Genomic Clones. A human DGK cDNA fragment was used as a probe to screen a murine testis λgt11 cDNA library (CLONTECH). One 1.1-kb clone with nearly the full-length coding sequence was used to screen a murine 129SVJ Fix II genomic library (Stratagene) as described (24). Positive clones were subcloned into pBluescript II SK (+), and the genomic organization was analyzed by a combination of restriction mapping, Southern blotting, subcloning, and automated sequencing (24). A full-length cDNA clone was generated by using PCR from the genomic clone and then it was subcloned into pcDNA3 (Invitrogen) for expression of the protein in mammalian cells.

Tissue Culture, Transfection, and Analysis of DGK Activity. COS-7 cells were cultured and transfected (25), and *in vitro* DGK assays using the cell lysates were performed (13).

This paper was submitted directly (Track II) to the PNAS office.

Abbreviations: ECS, electroconvulsive shock; EPSP, excitatory postsynaptic potential; FFA, free fatty acid; HFS, high-frequency stimulation; LTP, long-term potentiation; mGluR, metabotropic glutamate receptor; PA, phosphatidic acid; PAF, platelet-activating factor; PIP_2, phosphatidylinositol 4,5-bisphosphate.

‡To whom reprint requests should be addressed. S.M.P., Huntsman Cancer Institute, University of Utah, Salt Lake City, UT 84112; or N.G.B., Neuroscience Center, Louisiana State University Health Sciences Center, 2020 Gravier Street, Suite D, New Orleans, LA 70112. E-mail: nbazan@lsuhsc.edu.

The publication costs of this article were defrayed in part by page charge payment. This article must therefore be hereby marked "*advertisement*" in accordance with 18 U.S.C. §1734 solely to indicate this fact.

www.pnas.org/cgi/doi/10.1073/pnas.081536298

Analysis of Multiple-Tissue Northern Blot. A murine multiple-tissue Northern blot (CLONTECH) was probed with a ^{32}P-labeled fragment of murine DGK corresponding to nucleotides 532-1580 by using ExpressHyb (CLONTECH) according to the manufacturer's protocol.

Histology and *in Situ* Hybridization. Probes for *in situ* hybridization corresponded to nucleotides 532-1580 of murine DGK and nucleotides 192–791 of murine glyceraldehyde-3-phosphate dehydrogenase. Sections were deparaffinized, rehydrated, and incubated at room temperature for 30 min with proteinase K (6 μg/ml) and then for 10 min in 0.25% acetic anhydride/0.1 M triethanolamine. Sections were dehydrated and hybridized for 16 h at 58°C with digoxigenin-labeled sense or antisense RNA probes (1 μg/ml) in a solution of 10% dextran sulfate, 50% formamide, 100 mM DTT, 0.3 M NaCl, 5 mM EDTA, 1× Denhardt's solution (0.02% polyvinylpyrrolidone/0.02% Ficoll/0.02% BSA), yeast tRNA (500 μg/ml), and 20 mM Tris·HCl (pH 7.5). Sections were washed for 1 h at room temperature in 4× SSC/10 mM DTT and for 30 min at 58°C in 50% formamide/1× SSC/10 mM DTT. After digestion with RNase A (10 μg/ml) for 30 min at 37°C, sections were washed 15 min in 2× SSC, 15 min in 0.1× SSC, and then 2 min in buffer 1 (100 mM maleic acid/150 mM NaCl, pH 7.5). Sections then were incubated at room temperature for 30 min in buffer 1/10% normal sheep serum, then with anti-digoxigenin alkaline phosphatase conjugate (1:500 dilution in buffer 1/10% normal sheep serum/0.3% Triton X-100) for 2 h, and were washed for three 10-min periods in buffer 1 and for 2 min in buffer 3 (100 mM NaCl/0 mM $MgCl_2$/100 mM Tris·HCl, pH 9.5). Signals were detected after incubation in nitroblue tetrazolium (338 μg/ml)/5-bromo-4-chloro-3-indolyl phosphate (175 μg/ml) in buffer 3 for several hours to 1 day.

Construction of the DGK Targeting Vector and Screen for Targeted Embryonic Stem (ES) Cells. A DGK targeting vector was produced by replacing exon 1 of the DGK gene with a neomycin-resistance (*neo*^{r}) cassette, which provided for positive selection. This and flanking genomic DNAs were subcloned into the phage targeting vector MDASHII-2TK254 (Kirk Thomas, University of Utah), placing it between two thymidine kinase genes for negative selection. The linearized vector was electroporated into R1 ES cells, which then were screened by positive–negative selection (26). To screen ES cell clones for homologous recombination, DNA from selected ES cell lines was digested with *Xba*I and subjected to Southern blot analysis using probe A (24). Of 72 selected clones, 17 (23%) contained the targeted allele. The homologous recombinant clones (with a 10.5-kb, rather than a 15.0-kb, fragment) were then injected into C57/BL6 blastocysts that were injected into uteri of pseudopregnant C57/BL6 females. Resulting male chimeric mice were back-crossed with BL/6 females and heterozygous mutants were identified by genomic Southern blotting and PCR by using tail DNA as described below.

Genotyping by PCR and Southern Blotting. Genotyping was performed at the time of birth and again the day of the experiment 2–3 months later. Mouse tail (1–2 cm) was digested [5 mM EDTA/200 mM NaCl/100 mM Tris·HCl, pH 8.0/0.2% SDS/proteinase K (0.5 mg/ml)/RNase A (12.5 g/ml)] overnight in a water bath at 55°C. The DNA was extracted with phenol/chloroform/isoamyl alcohol, 25:24:1 (vol/vol), washed twice in chloroform/isoamyl alcohol, 26:4 (vol/vol), and precipitated with 1:1 isopropanol. Pellets were resuspended in Tris/EDTA (pH 8.0) and heated for 2 h at 65°C. Southern blotting was performed as described above. Each PCR mixture contained 0.5 μl of DNA, 1× *Pfu* Turbo buffer, all four dNTPs (each at η2 mM), 2.5 μM forward and reverse primers, 1% Tween-20, water, and *Pfu* Turbo DNA polymerase (2.5 unit) in a total volume of 25 μl. A forward primer from a region on the 5′ side of exon 1 (5′-AGAGAGGCACGGGCGAGGCTC-3′) and a reverse primer in exon 1 (5′-GCGCGACCGCTGCAGGCTACA-3′) were used to amplify the wild-type allele. The same forward primer and a reverse primer from the *neo*^{r} cassette (5′-CAGGACGTTGGGGGCACCGCCT-3′) were used to identify the mutant allelle. Homozygous product size was 242 bp and the wild-type product size was 344 bp. Reactions were carried out at 94°C for 5 min, 94°C for 1.0 min, 65°C for 1.5 min, and 72°C for 1.5 min for 35 cycles and then 72°C for 5 min.

ECS. Two- to 3-month-old mice (20–25 g, male/female) were acutely implanted with two platinum electrodes under the scalp (parallel, 1 cm apart). A single stimulation train of square pulses was delivered at 50 V dc and 0.5-msec pulse duration with a frequency of 100 pulses per second, a train duration of 200 msec, and a train rate of 0.750 train per second (27). This stimulation evoked, in wild-type mice, a tonic seizure lasting 15–20 sec, followed by a clonic seizure. Differences in the behavioral response to ECS among wild-type, heterozygous (+/−), and homozygous (−/−) DGKε mice are summarized in Fig. 4.

Lipid Analysis. Mice were killed by high-frequency head-focused microwave irradiation, their heads were cooled quickly in ice-cold water, and the brains were dissected. Lipids from the right cerebral cortex were extracted with hexane/isopropanol, 3:2 (vol/vol), for the analysis of free fatty acids (FFA) and DAG. Polyphosphoinositides (PPI) were extracted from the left cerebral cortex with acidified chloroform/methanol. Lipid classes by TLC were isolated and their acyl groups were analyzed by gas liquid chromatography (28).

Electrophysiological Recordings. Hippocampal slices were prepared from either sex of DGK-deficient mice and age-matched control mice, as described (4), and individual dentate granular cells were visualized with a Zeiss Axioskop microscope.

Whole-cell patch-clamp recordings were made with an Axoclamp-2B patch-clamp amplifier in bridge mode as described (4). Data were acquired (25 kHz, filtered at 1 kHz) by using a DigiData 1200 interface and PCLAMP 7.01 software (Axon Instruments, Foster City, CA). Excitatory postsynaptic potentials (EPSPs) in response to stimulation of the perforant path were recorded at a frequency of 0.05 Hz and the amplitude range of the evoked EPSPs was always adjusted to 2–6 mV (<30% threshold for generating an action potential). LTP in the perforant path was induced by high-frequency stimulation (HFS) consisting of eight trains, each of eight pulses at 200 Hz with an intertrain interval of 2 sec, as described (29). LTP was operationally defined as >20% increase above baseline for the amplitude of ESPSs from 26 to 30 min after HFS.

Statistical Analysis. Data are the mean ± SEM. Statistical analysis was performed with the unpaired Student's t test. One-way ANOVA with Fisher's PLSD post hoc was used for statistical comparison when appropriate. Statistical analysis of the frequency of the behavioral responses to ECS (see Fig. 4) was done with the χ^2 test. Differences were considered significant when $P < 0.05$.

Results

Cloning and Characterization of Murine DGK. Because human DGK is expressed predominantly in testis, a murine testis cDNA library was screened with a human DGK cDNA fragment as a probe. A 1.1-kb partial clone was obtained and used to screen a murine genomic library. With clones obtained from this screen, the full-length cDNA was secured by PCR. Murine DGK is a 564-aa protein with a calculated molecular mass of 64 kDa. Alignment of the murine and human orthologs revealed 91% amino acid identity. Like its human counterpart, murine DGK displayed high selectivity for 20:4-DAG when compared with oleoyl-DAG (10.8 ± 1.3-fold higher, $n = 3$) and other DAG species (data not shown). To determine the distribution of murine DGK, we probed a multiple-

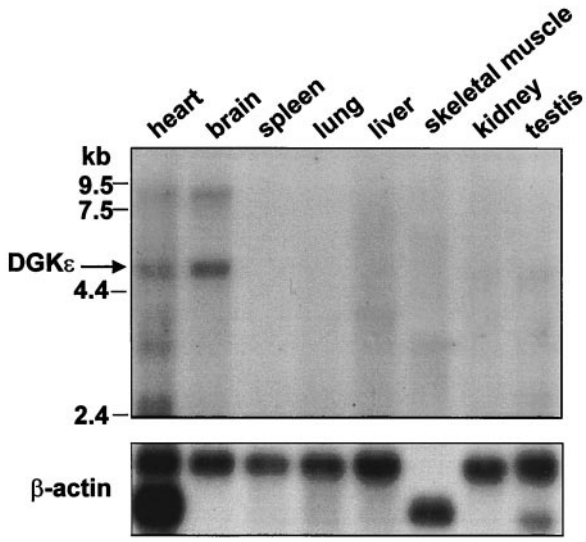

Fig. 1. DGKε mRNA distribution in murine tissues by Northern blot analysis. Brain and heart tissues show the highest constitutive expression levels of 5- and 8-kb DGKε; testis show only the 5-kb band.

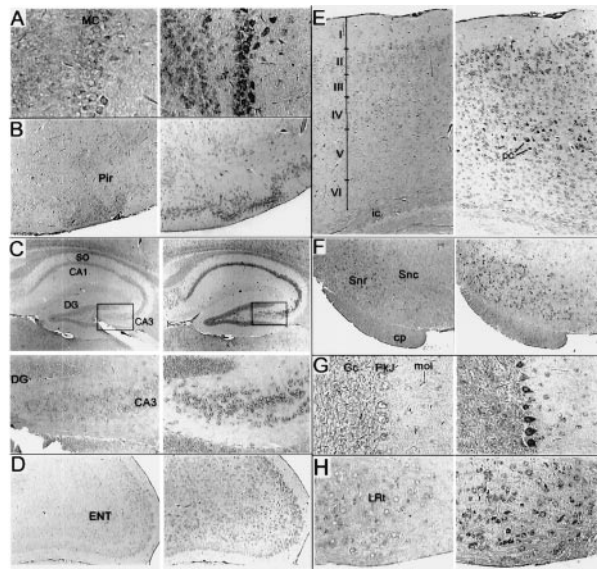

Fig. 2. Distribution of DGKε in the mouse brain as measured by *in situ* hybridization. Adjacent sagital sections were hybridized with sense (*Left*) or antisense (*Right*) digoxigenin-labeled probe prepared from a 0.9-kb *Eco*RI fragment of murine DGKε. (*A*) Staining of the olfactory bulb was most notable in mytrial cells (MC; ×150) and to a lesser extent in the granular cells. (*B*) Staining was notable in the piriform cortex (Pir; ×60) but was not prevalent in adjacent cortical structures including the insular cortex (data not shown). (*C*) In the hippocampus (×40, and boxed regions at ×160, *Lower*), intense signal in the pyramidal cells of CA3 but only weak staining of dentate granular (DG) cells. Pyramidal cells of CA1 were labeled throughout, but no signal in the stratum oriens (so) and only inconsistent staining of cells in other hippocampal regions was observed. (*D*) Prominent signal for DGKε RNA detected in the entorhinal cortex (ENT; ×60) and especially cells of the outer layers. (*E*) Staining of the medial occipital (neo) cortex (×80) in all layers but was most prominent in the pyramidal cells (pc) of layer 5. Definition of the layers was based upon adjacent sections counterstained with Giemsa (data not shown). No staining of cells over background in the internal capsule (ic) was detected. Staining of cells in the thalamus or in structures of the basal ganglia was occasional or absent, except in *F* (×60) for the substantia nigra reticulata (Snr). Staining of cells in the substantia nigra compacta (Snc) was present but inconsistent. The cerebral peduncle (cp) is identified. (*G*) In the cerebellum (×150), staining was most intense in Purkinje cells (Pkj) but could be identified above background in cerebellar granular cells (Gc) and cells of the layer molecular (mol). Staining of cells throughout the hindbrain and Pons was observed including trigeminal nuclei and the superior olive (data not shown). (*H*) Staining was particularly intense in the lateral reticular nucleus (LNR; ×150).

tissue Northern blot and found specific 5-kb and 8-kb bands, most highly expressed in brain and heart (Fig. 1). A 5-kb band was also apparent in testis. In contrast, human DGK was highly expressed in testis and barely detectable in other tissues (13). However, Kohyama-Koganeya *et al.* (30) noted that rat DGK mRNA was also enriched in brain and heart. A subsequent reprobe of a human multiple-tissue Northern blot with a different fragment of DGK as a probe detected signals in the brain and heart (data not shown), confirming that the bands observed on the murine blot represent DGK mRNA. DGK sublocalization in murine brain tissue, by *in situ* hybridization, revealed the highest signals in Purkinje cells of the cerebellum, pyramidal cells of the hippocampus, mitral cells of the olfactory bulb, and neurons of the substantia nigra (Fig. 2). This distribution corresponded well with that reported for rat DGK (30). Lower expression of DGK in neurons of the thalamus, superior olive, and lateral reticular nucleus was also detected.

Generation of DGKε-Deficient Mice. The C1 domains of DGK were necessary for its activity, because deleting them rendered DGK inactive (data not shown). Exon 1 of the murine DGKε gene encoded the initiation methionine and the first and most of the second C1 domains, so a vector for targeted deletion that replaced this exon with a neomycin-resistance insert was designed (Fig. 3*A*). Properly targeted, the deletion construct should result in a null mutation. Heterozygous mice (DGK$\varepsilon^{+/-}$) were viable and fertile and were intercrossed to obtain DGK$\varepsilon^{-/-}$ mice. The genotype of the offspring was determined by Southern blotting (Fig. 3*C*), where targeted deletion resulted in a 10.5-kb band instead of a 15-kb band. These results were verified by a PCR screen (data not shown). A Mendelian pattern of inheritance of the targeted allele with a normal gender distribution was found, indicating that the deletion did not cause embryonic lethality. Homozygous DGKε null mice appeared normal and reproduced and behaved normally. No gross or histological abnormalities in major organs, including the brain, were found in DGK$\varepsilon^{-/-}$ mice.

Behavioral Responses to ECS in DGKε Knockout Mice. Because PPI signaling by mGluRs is stimulated by ECS (8), the behavioral response to ECS of DGK$\varepsilon^{-/-}$ mice was studied. These mice displayed shorter tonic seizures compared with DGK$\varepsilon^{+/+}$ mice, with only 24% of the animals having sustained tonic seizure >15 sec and 50% developing a 10- to 15-sec tonic seizure (Fig. 4). After the clonic phase, DGK$\varepsilon^{-/-}$ mice recovered faster than DGK$\varepsilon^{+/+}$ mice, within 1–3 min after ECS. Approximately 28% of DGK$\varepsilon^{-/-}$ mice jumped immediately after stimulation, developing a very short tonic seizure (7–8 sec, 21%) after a 3-sec delay or no tonic seizure (7%). The length of the tonic seizure in heterozygous mice for the null allele (DGK$\varepsilon^{+/-}$) was intermediate between DGK$\varepsilon^{+/+}$ and DGK$\varepsilon^{-/-}$ mice, whereas their recovery was very slow as observed in DGK$\varepsilon^{+/+}$ mice. No differences in behavioral responses to ECS were observed between males and females.

DGK$\varepsilon^{-/-}$ Mice Display Decreased ECS-Induced Polyphosphoinositides Degradation and Lower Accumulation of DAG and Free 20:4. PPI content in cerebral cortex was unchanged in DGK$\varepsilon^{-/-}$ mice compared with DGK$\varepsilon^{+/+}$ mice under resting conditions, except for a decrease of 20:4-PIP_2 and a higher content of docosahexaenoic acid (22:6n-3) in PIP and PIP_2. ($P < 0.01$; Fig. 5). Stearoyl (18:0)- and 20:4-PIP_2, as expected, rapidly decreased in DGK$\varepsilon^{+/+}$ mice after ECS, but no significant changes were observed in DGK$\varepsilon^{-/-}$ mice (Fig. 5). In contrast, 18:0- and 20:4-PIP were decreased only in DGK$\varepsilon^{-/-}$ mice. 22:6-PIP, on the other hand, showed lower content 30 sec and 1 min after ECS only in DGK$\varepsilon^{-/-}$ mice.

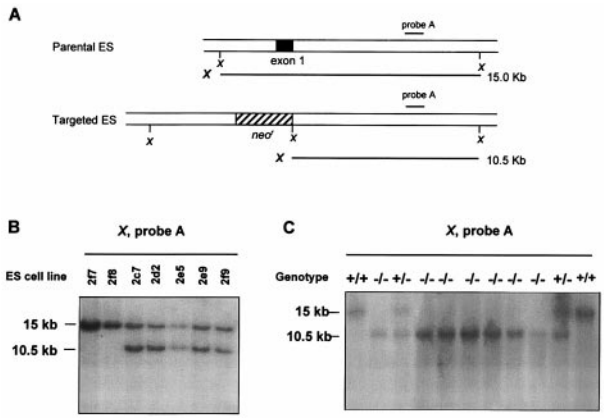

Fig. 3. Strategy for targeted disruption of the DGKε gene in the R1 ES cell line and C57/BL6 mice. (*A*) Parental and targeted DNA fragments after digestion with *Xba*I in ES cell lines. (*B*) Southern blot analysis of selected ES cell lines. Untargeted cell lines were 2f7 and 2f8. Targeted cell lines were 2c7, 2d2, 2e5, 2e9, and 2f9. (*C*) Southern blot analysis of wild-type and heterozygous mutants by using tail DNA extracts. The 15-kb band is wild type, and the 10.5-kb band is the targeted deletion of DGKε.

DAG resting levels varied among DGK$\varepsilon^{-/-}$ mice. From the 16 DGK$\varepsilon^{-/-}$ mice analyzed (mean ± SEM, 108 ± 21 nmol per mg of lipid phosphate), five showed relatively high content of DAG (n = 10; DGK$\varepsilon^{+/+}$ mice, 110 ± 15 nmol per mg of lipid phosphate; DGK$\varepsilon^{-/-}$: 217 ± 30 nmol per mg of lipid phosphate; $P < 0.02$) and 11 mice displayed very low DAG content (57 ± 6 nmol per mg of lipid phosphate, $P < 0.02$) compared with DGK$\varepsilon^{+/+}$ mice. However, the acyl group composition remained unchanged in all of the DGK$\varepsilon^{-/-}$ mice studied. No differences were observed in the resting FFA pool size and composition, including free 20:4.

FFA and DAG content in the cortex from DGK$\varepsilon^{-/-}$ and DGK$\varepsilon^{+/+}$ mice after ECS are shown in Fig. 6. Within 30 sec after ECS, wild-type mice displayed a 2.2-fold increase in DAG, decreasing thereafter and reaching basal values by 3 min. All acyl groups contributed to the transient enlargement of the DAG pool, 20:4-DAG displaying the slower recovery and remaining 2.4-fold above the basal level by 5 min. Accumulation of DAG was lower in DGK$\varepsilon^{-/-}$ mice (1.4-fold by 30 sec) recovering basal values by 1 min after ECS. Only 18:0- and 20:4-DAG were significantly increased by 30 sec. From the 25 DGK$\varepsilon^{-/-}$ mice subjected to ECS, 44% did not show changes in DAG and FFA and were not included in Fig. 6. Interestingly, this group includes all mice that did not develop tonic seizures and some that showed 10- to 12-sec seizures.

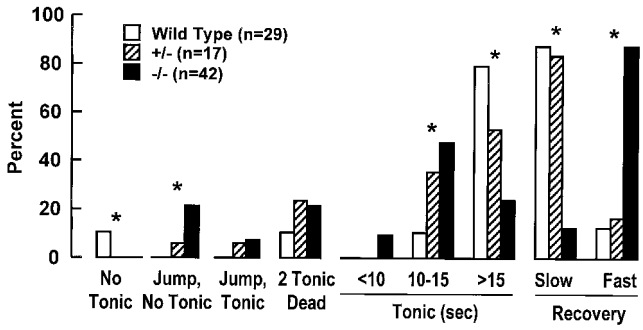

Fig. 4. Behavioral responses of ECS-induced seizures in wild-type, heterozygous, and homozygous DGKε mice. Wild-type mice display a tonic seizure lasting 15–20 sec, followed by clonic seizure, remaining lying on their side and recovering their posture by 3–4 min after ECS (slow recovery). χ^2 test was used for the statistical analysis of the data. * denotes significant differences for all three phenotypes in the frequency of the behavioral response to ECS ($P < 0.05$).

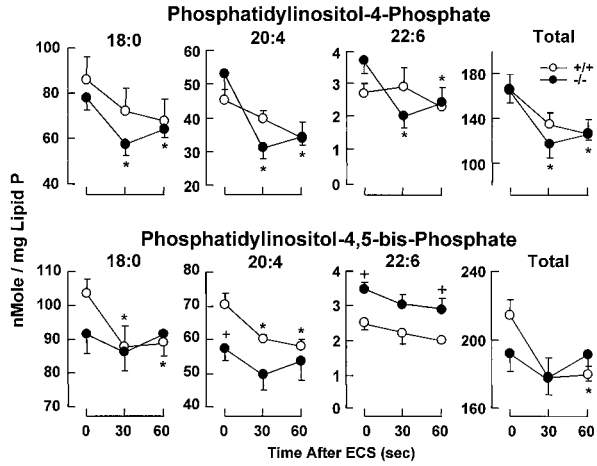

Fig. 5. ECS-induced degradation of PIP_2 is decreased in the DGK$\varepsilon^{-/-}$ mice. Mean values ± SEM are shown (n = 4–6). Statistically significant differences (Student's t test, $P < 0.05$) are indicated: *, with respect to control (0 time); +, DGK$\varepsilon^{-/-}$ mice vs. DGK$\varepsilon^{+/+}$ mice.

The FFA pool was increased in DGK$\varepsilon^{+/+}$ mice by 3.8- and 6-fold at 30 sec and 1 min after ECS, respectively, decreasing thereafter but remaining 3.2-fold above the basal level by 5 min. In contrast, in DGK$\varepsilon^{-/-}$ mice, FFA only reached a 2.1-fold increase by 30 sec after ECS, remaining unchanged thereafter. All fatty acids reached values significantly lower than DGK$\varepsilon^{+/+}$ mice after ECS, 18:0 and 20:4 displaying the greatest differences. Free 20:4 and 18:1 displayed the faster recovery toward basal values in DGK$\varepsilon^{+/+}$ mice but remained at the same level reached by 30 sec after ECS in DGK$\varepsilon^{-/-}$ mice.

Induction of LTP Is Attenuated in the Perforant Path Dentate Gyrus Cell Synapses of DGKε-Deficient Mice. Synaptic transmission and plasticity were examined in dentate granular cells of DGKε-deficient mice and their age-matched normal controls. There were no abnormalities in basic membrane properties, including resting membrane potential, input resistance, and action potential generation (8–10 spikes per burst) in cells from hippocampal slices from enzyme-deficient mice. As indicated in Fig. 7, however, the potentiation of EPSP amplitude by HFS was significantly reduced in cells from DGK$\varepsilon^{-/-}$ mice (potentiation, mean ± SEM, 135 ± 11% of

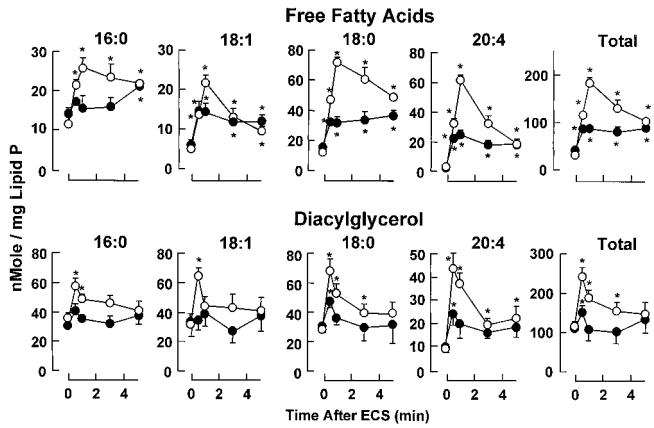

Fig. 6. ECS-induced accumulation of FFA and DAG in wild-type and DGK$\varepsilon^{-/-}$ mice. Mean values ± SEM are shown. Basal values (time 0) are the average of 16 samples. Other time points are from 5–8 individual samples. * denotes values significantly different from basal ($P < 0.05$, Student's t test).

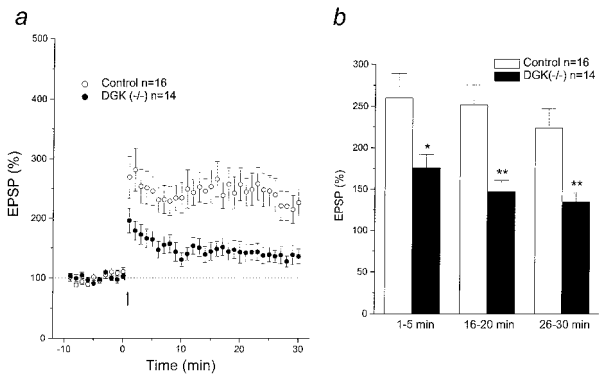

Fig. 7. Reduced LTP in hippocampal perforant path–dentate gyrus neurons of mice deficient in the DGKε. (*a*) Time course and extent of LTP induction after HFS (arrow) in control and DGK$\varepsilon^{-/-}$ mice. EPSP amplitude was normalized as percent of average baseline EPSP amplitude. (*b*) Mean potentiation of EPSP calculated by the average EPSP amplitude at 1–5 min, 16–20 min, and 26–30 min after HFS plotted as percent of baseline. Data are mean ± SEM. *, $P < 0.05$; **, $P < 0.01$.

baseline from 26 to 30 min after HFS) when compared with that in the DGK$\varepsilon^{+/+}$ mice (224 ± 23%).

Discussion

In the present study, we have cloned and characterized the murine DGKε, showing its selectivity for 20:4-DAG phosphorylation and its high expression in brain. By using a targeted deletion of the DGKε, we demonstrated decreased behavioral responses to ECS correlated with decreased accumulation of 20:4-DAG, free 20:4, and PIP_2 degradation during seizures. Moreover, DGKε deficiency resulted in attenuated LTP in hippocampal dentate gyrus neurons.

DGKε Knockout Mice. We generated mice with disrupted DGKε alleles by gene targeting. Murine DGKε displayed similar selectivity for 20:4-DAG as human DGKε (13); thus, the enzymatic selectivity of DGKε seems to be conserved in mammals. This 20:4-DAG-specific DGK may be significant in terminating signals transduced through 20:4-DAG generated in the PIP_2 cycle. However, the tissue distribution patterns of murine and human DGKε are different, as demonstrated by Northern blotting in which murine DGKε was primarily expressed in brain and human DGKε was predominantly in testis (13). This difference may be caused by distinct specificity of probes used. The probe used in our previous study was prepared from the 3′ untranslated region of DGKε cDNA rather than the coding region, used herein. In fact, the specific mRNA band of human DGKε was also detected in brain and heart when hybridized with a probe prepared from the coding region of its cDNA in tissue Northern blotting. Alternatively, this difference may reflect the involvement of murine and human DGKε in different signaling pathways. The cellular distribution of murine DGKε in brain by *in situ* hybridization was similar to that of the mGluR1 in cerebellar Purkinje cells, mitral cells of the olfactory bulb, hippocampal interneurons and neurons of the thalamus and substantia nigra (31, 32). G protein-coupled mGluR1 leads to PIP_2 hydrolysis catalyzed by PLC and the subsequent activation of PKCβ.

Down-Regulation of 20:4–Inositol Lipid Signaling and Resistance to ECS-Induced Seizure. Because ECS and ischemia activate the PLC-mediated release of 20:4-DAG (8, 33, 34), we investigated whether deficiency of DGKε, which terminates 20:4-DAG signals, would affect the seizure response to ECS. We found that male and female DGKε-deficient mice were more resistant to ECS, displaying shorter tonic seizures and faster recovery than DGK$\varepsilon^{+/+}$ mice. This behavioral response was paralleled by lower degradation of brain PIP_2 and lower accumulation of DAG and FFA after ECS. Moreover, DGK$\varepsilon^{-/-}$ mice recovered DAG basal levels within 1 min after ECS, but a more sustained accumulation was observed in DGK$\varepsilon^{+/+}$ mice.

Although resting levels of PIP and PIP_2 were similar in cerebral cortex from DGK$\varepsilon^{-/-}$ and DGK$\varepsilon^{+/+}$ mice, some changes were detected. Neuronal PPI is maintained by *de novo* synthesis via PA, whereas the DAG–DGKε pathway contributes to their resynthesis after synaptic activity-induced PIP_2 degradation. Activation of the mGluRs regulates the operation of this cycle through PLC. In DGK$\varepsilon^{-/-}$mice, only 20:4-PIP_2 displayed decreased resting levels. Therefore, despite the deficiency in DGKε selective for 20:4-DAG phosphorylation, other DAG kinase(s) and/or the *de novo* synthesis pathway may partly compensate to generate 20:4-PA that, in turn, is channeled to inositol lipids. Moreover, DGK$\varepsilon^{-/-}$ mice did not show enrichment in 20:4-DAG and only 31% of the animals displayed higher resting levels of total DAG as compared with DGK$\varepsilon^{+/+}$ mice. Likely, the resting 20:4-DAG pool of the PPI pathway is very small compared with the pool of 20:4-DAG linked to the turnover of other phospholipids and, therefore, changes may be masked by the total DAG pool.

The ECS-induced 18:0- and 20:4-DAG accumulation in the cerebral cortex by 30 sec was lower in DGK$\varepsilon^{-/-}$ mice than in DGK$\varepsilon^{+/+}$ mice. However, the removal of DAG showed similar kinetics to that in DGK$\varepsilon^{+/+}$ mice, suggesting that, even after stimulation, other DGK(s) may compensate for the DGKε deficiency. The DAG pathway is terminated by DGK through its phosphorylation to PA and/or by DAG lipases with the generation of FFA (9). However, the rapid removal of DAG in DGK$\varepsilon^{-/-}$ mice was not paralleled by a further increase in FFA, supporting the notion that DGKs, rather than DAG lipases, other than DGKε are involved in the efficient removal of DAG after ECS in DGK$\varepsilon^{-/-}$ mice.

Interestingly, DGK$\varepsilon^{-/-}$ mice displayed very low PIP_2 degradation after ECS, suggesting impairments in mGluR function linked to G proteins and PLC activation. It is possible that to cope with the deficiency of the DGKε, adaptative and/or compensatory changes are developed. This may include a persistent PKC binding to the membrane in close association with the mGluR–G protein–PLC complex, where 20:4-DAG accumulates. Because PKC controls the PPI cycle by feedback inhibition of PLC (6), this sustained translocation will inhibit the PPI–PLC signaling, as reflected in the low ECS-induced 20:4-DAG release.

In DGK$\varepsilon^{-/-}$ mice, a significant decrease of 18:0- and 20:4-PIP not observed in DGK$\varepsilon^{+/+}$ mice took place after ECS. Because stimulation activates degradation and resynthesis of inositol lipids, the levels of PIP and PIP_2 reflect the balance of these two pathways. In DGK$\varepsilon^{+/+}$ mice, degradation of PIP_2 occurs at a faster rate than its replenishment from PIP by PIP 4-phosphate 5-kinase, while PIP is being replenished through the DAG–PA–phosphatidylinositol pathway. This results in a decrease of PIP_2 and no detectable changes in PIP. In DGK$\varepsilon^{-/-}$ mice, the decrease observed in PIP may indicate its active phosphorylation to PIP_2 and its slower replenishment from the DAG–DGK$\varepsilon^{-/-}$ pathway. Because type I PIP 4-phosphate 5-kinase ε is highly expressed in the brain and greatly stimulated by PA (35, 36), deficiency of DGKε will likely not force PIP_2 resynthesis. Therefore, other metabolic dysfunctions to be considered in DGKε deficiency are the PIP degradation by PLC and/or its dephosphorylation to phosphatidylinositol.

In DGK$\varepsilon^{+/+}$ mice, there was also accumulation of 16:0- and 18:1-DAG after ECS, while levels of 16:0- and 18:1-PIP_2 remained unchanged (data not shown). These changes are consistent with degradation of other phospholipids through a PLD pathway that contributes to the sustained accumulation of DAG (2). In DGK$\varepsilon^{-/-}$ mice, however, no change in 16:0- and 18:1-DAG was observed. Thus, the disruption of the inositol lipid cycle and, therefore, the lack of DAG-stimulated PKC-mediated activation of PLD may lead to the loss of PLD response to stimulation (37).

These results suggest impairments in multiple signaling pathway response to ECS that, in turn, may contribute to the observed fast recovery of DGK$\varepsilon^{-/-}$ mice from tonic–clonic seizures.

The magnitude of free 20:4 and other FFA accumulation after ECS in DGK$\varepsilon^{-/-}$ mice compared with DGK$\varepsilon^{+/+}$ mice unveiled potential alterations in the calcium-dependent $cPLA_2$ pathway. Degradation of 18:0- and 20:4-DAG generated from PIP_2 after ECS may contribute to the FFA pool (2). However, the release of 20:4 after ECS, when PIP_2 levels start to recover, implicates the activation of $cPLA_2$ targeting with high selectivity of 20:4-phospholipids (4). NMDA receptor activation leads to calcium influx and $cPLA_2$ activation (2). The intracellular mobilization of calcium by IP_3 also contributes to sustained activation of $cPLA_2$. The $cPLA_2$ signaling has a profound impact in responses to stimulation because 20:4 by itself, and eicosanoids generated by COX-1–COX-2, are involved in the modulation of synaptic activity (2). Moreover, $cPLA_2$ generates lyso-PAF, the precursor of PAF, a neuromodulator of LTP (38) that stimulates glutamate release from presynaptic terminals (39) and activates transcription of genes (9, 27, 40). In cultures of hippocampal neurons from DGK$\varepsilon^{-/-}$ mice, glutamate stimulation resulted in lower accumulation of intracellular Ca^{2+} compared with cells from DGK$\varepsilon^{+/+}$ mice (unpublished results). In this context, it is relevant that sustained increase in intracellular Ca^{2+} appears to be required for $cPLA_2$ translocation to the membrane and full enzymatic activity (41). Decreased activity of $cPLA_2$ and consequently lower release of 20:4 and PAF production in DGK$\varepsilon^{-/-}$ mice are also supported by the observation that LTP is attenuated in perforant path–dentate granular cell synapses.

In summary, changes in lipid messengers generated in the cortex of DGK$\varepsilon^{-/-}$ mice after one ECS were complex and suggestive of alterations in different signaling pathways (i.e., PLA_2, PLC, and PLD) triggered by the deficiency in DGKε. The lack of the DGKε should lead to a higher accumulation of 20:4-DAG after ECS compared with DGK$\varepsilon^{+/+}$ mice. In contrast, changes were of much lower magnitude as a result of lower production of 20:4-DAG through PIP_2-PLC and reflected in the lower changes detected in 20:4-PIP_2 compared with DGK$\varepsilon^{+/+}$ mice. Deficiency in the PLA_2 and PLC signaling by ECS leads to impaired release of messengers (i.e., 20:4, eicosanoids, PAF, DAG). These messengers are involved in the potentiation of excitatory neurotransmission favoring further glutamate release and a more efficient and sustained glutamate signaling in postsynaptic neurons (2). Thus, the observed changes may underlie the higher resistance to seizure and faster recovery observed in DGK$\varepsilon^{-/-}$ mice.

Attenuated LTP in DGK$\varepsilon^{-/-}$ Mice. HFS-induced LTP is reduced in perforant path–dentate granular cell synapses in DGKε-deficient mice compared with that of wild-type mice. These mice displayed lower release of 20:4 induced by ECS, suggestive of lower $cPLA_2$ activity necessary for PAF synthesis. The attenuation of LTP in DGK$\varepsilon^{-/-}$ mice may, therefore, be the consequence of diminished PAF synthesis directly involved in modulating excitatory synaptic activity (38, 39). However, low production of other 20:4-inositol lipid-derived signaling molecules also may contribute to alterations in synaptic plasticity. In addition, the hippocampal dentate gyrus is of significance for learning and memory and for epileptogenesis. Thus, alterations in the 20:4–inositol lipid cycle take place in limbic structures that display high DGKε expression and may contribute to synaptic dysfunction and pathology.

Conclusion. In this study, we have cloned and characterized the murine DGKε. The enzyme displays selectivity for 20:4-DAG and is highly expressed in different areas of the brain, including Purkinje cells in the cerebellum, hippocampal interneurons, and the pyramidal neurons in the CA3 region of the hippocampus. We generated mice with targeted disruption of the DGKε and show that a DGKε deficiency affects multiple signaling including the PIP_2–PLC and the $cPLA_2$–20:4 pathways. This, in turn, leads to higher resistance of neurons to seizures and attenuation of LTP. Moreover, higher resistance to ischemic neuronal damage may also occur. Although DGKε is the sole cloned mammalian DGK displaying high selectivity for 20:4 lipids, it is possible that the function of DGKε *in vivo* can be compensated, at least in part, by other DGKs when DGKε is inactivated. Deficiency of DGKε, selective for 20:4-DAG, has allowed us to identify synaptic signaling activated during epileptogenesis and contributing to seizure development. The genetic approach used herein demonstrates avenues for exploration of inositol lipid signaling, critical in generating potent messengers at the synapse.

We thank Mattie Hardy and Nilda Parkins (LSUHSC), Margaret Robinson (University of Utah Cancer Center Core Sequencing Facility), Bob Schackmann (University of Utah Peptide/DNA User Facility; supported by Grant CA42014), Bradley Preston (Transgenic/Gene Targeting Mouse Lab, University of Utah), Kelley Murphy, and Katrina Anderson for expert assistance. We are grateful to Dr. Kirk Thomas and Dr. Scott Rogers (University of Utah) for helpful contributions and discussions. This work was supported by Grants CA59548 and R01-NS-23002 from the National Institutes of Health.

1. Bazan, N. G. (1989) *Ann. N.Y. Acad. Sci.* **559,** 1–16.
2. Bazan, N. G., Rodriguez de Turco, E. B. & Allan, G. (1995) *J. Neurotrauma* **12,** 791–814.
3. Bazan, N. G. & Allan, G. (1998) in *Cerebrovascular Disease, Pathophysiology, Diagnosis, and Management*, eds. Ginsberg, M. D. & Bogousslavsky, J. (Blackwell Scientific, Oxford), pp. 532–555.
4. Chen, C., Magee, J. C., Marcheselli, V., Hardy, M. & Bazan, N. G. (2001) *J. Neurophysiol.* **85,** 384–390.
5. Conn, P. J. & Pin, J. P. (1997) *Annu. Rev. Pharmacol. Toxicol.* **37,** 205–237.
6. Nishizuka, Y. (1995) *FASEB J.* **9,** 489–496.
7. Hodgkin, M. N., Pettitt, T. R., Martin, A., Michell, R. H., Pemberton, A. J. & Wakelam, M. J. (1998) *Trends Biochem. Sci.* **23,** 200–204.
8. Reddy, T. S. & Bazan, N. G. (1987) *J. Neurosci. Res.* **18,** 449–455.
9. Bazan, N. G., Allan, G. & Rodriguez de Turco, E. B. (1993) *Prog. Brain Res.* **96,** 247–257.
10. Wakelam, M. J. (1998) *Biochim. Biophys. Acta* **1436,** 117–126.
11. Pettitt, T. R. & Wakelam, M. J. O. (1999) *J. Biol. Chem.* **274,** 36181–36186.
12. Prescott, S. M. & Majerus, P. W. (1981) *J. Biol. Chem.* **256,** 579–582.
13. Tang, W., Bunting, M., Zimmerman, G. A., McIntyre, T. M. & Prescott, S. M. (1996) *J. Biol. Chem.* **271,** 10237–10241.
14. Topham, M. K. & Prescott, S. M. (1999) *J. Biol. Chem.* **274,** 11447–11450.
15. Abeliovich, A., Chen, C., Goda, Y., Silva, A. J., Stevens, C. F. & Tonegawa, S. (1993) *Cell* **75,** 1253–1262.
16. Abeliovich, A., Paylor, R., Chen, C., Kim, J. J., Wehner, J. M. M. & Tonegawa, S. (1993) *Cell* **75,** 1263–1271.
17. Nakanishi, S. (1994) *Neuron* **13,** 1031–1037.
18. Aiba, A., Chen, C., Herrup, K., Rosenmund, C., Steven, C. F. & Tonegawa, S. (1994) *Cell* **79,** 365–375.
19. Conquet, F., Bashir, Z. I., Davies, C. H., Daniel, H., Ferraguti, F., Bordi, F., Franz-Bacon, K., Reggiani, A., Matarese, V., Conde, F. *et al.* (1994) *Nature (London)* **372,** 237–243.
20. Wilsch, V. W., Behnisch, T., Jager, T., Reymann. K. G. & Balschun, D. (1998) *J. Neurosci.* **18,** 6071–6080.
21. Aiba, A., Kano, M., Chen, C., Stanton, M. E., Fox, G. D., Herrup, K., Zwingman, T. A. & Tonegawa, S. (1994) *Cell* **79,** 377–388.
22. Pacheco, M. A. & Jope, R. S. (1996) *Prog. Neurobiol.* **50,** 255–273.
23. Bordi, F. & Ugolini, A. (1999) *Prog. Neurobiol.* **59,** 55–79.
24. Tang, W., Bardien, S., Bhattacharya, S. S. & Prescott, S. M. (1999) *Gene* **239,** 185–92.
25. Bunting, M., Tang, W., Zimmerman, G. A., McIntyre, T. M. & Prescott, S. M. (1996) *J. Biol. Chem.* **271,** 10230–10236.
26. Thomas, K. R. & Capecchi, M. R. (1990) *Nature (London)* **346,** 847–850.
27. Marcheselli, V. L. & Bazan, N. G. (1994) *J. Neurosci.* **37,** 54–61.
28. Rodriguez de Turco, E. B., Deretic, D., Bazan, N. G. & Papermaster, D. S. (1997) *J. Biol. Chem.* **272,** 10491–10497.
29. Wang, Y., Wu, J., Rowan, M. & Anwyl, R. (1996) *J. Physiol. (London)* **495,** 755–767.
30. Kohyama-Koganeya, A., Watanabe, M. & Hotta, Y. (1997) *FEBS Lett.* **409,** 258–264.
31. Petralia, R. S., Wang, Y. X., Singh, S., Wu, C., Shi, L., Wei, J. & Wenthold, R. J. (1997) *J. Chem. Neuroanat.* **13,** 77–93.
32. Berthele, A., Laurie, D. J., Platzer, S., Zieglgansberger, W., Tolle, T. R. & Sommer, B. (1998) *Neuroscience* **85,** 733–749.
33. Aveldaño, M. I. & Bazan, N. G. (1975) *J. Neurochem.* **25,** 919–920.
34. Aveldaño de Caldironi, M. I. & Bazan, N. G. (1979) *Neurochem. Res.* **4,** 213–221.
35. Ishihara, H., Shibasaki, Y., Kizuki, N., Wada, T., Yazaki, Y., Asano, T. & Oka, Y. (1998) *J. Biol. Chem.* **273,** 8741–8748.
36. Anderson, R. A., Boronenkov, I. V., Doughman, S. D., Kunz, J. & Loijens, J. C. (1999) *J. Biol. Chem.* **274,** 9907–9910.
37. Exton, J. H. (1999) *Biochim. Biophys. Acta* **1439,** 121–131.
38. Kato, K., Clark, G. D., Bazan, N. G. & Zorumski, C. F. (1994) *Nature (London)* **367,** 175–179.
39. Clark, G. D., Happel, L. T., Zorumski, C. F. & Bazan, N. G. (1992) *Neuron* **9,** 1211–1216.
40. Squinto, S. P., Block, A. L., Braquet, P. & Bazan, N. G. (1989) *J. Neurosci. Res.* **24,** 558–566.
41. Hirabayashi, T., Kume, K., Hirose, K., Yokomizo, T., Iino, M., Itoh, H. & Shimizu, T. (1999) *J. Biol. Chem.* **274,** 5163–5169.